Magnetospheric and auroral activity during the 18 April 2002 sawtooth event

M. G. Henderson,[1] G. D. Reeves,[1] R. Skoug,[1] M. F. Thomsen,[1] M. H. Denton,[1] S. B. Mende,[2] T. J. Immel,[2] P. C. Brandt,[3] and H. J. Singer[4]

[1]   We examine the 18 April 2002 sawtooth event. We find that the strong magnetic field dipolarizations observed in association with each tooth are not global in occurrence but are rather confined to the nightside. In addition, we find that the flux increases are not globally dispersionless. Instead, each tooth is associated with a nonglobal, but wider-than-usual, dispersionless injection region that is consistent with the high Kp versions of the standard injection boundary model (which places the entire nightside segment of geosynchronous orbit tailward of the injection boundary for values of Kp above about 5). We also find evidence that at least one of the teeth was likely triggered by a pressure pulse. The auroral distribution shows a repeatable evolution in which a wide double-oval configuration gradually thins. Following this, a localized substorm-like brightening in the dusk to midnight sector occurs on the lower branch of the double oval which subsequently expands rapidly poleward and azimuthally. A new expanded double oval configuration emerges from this expansion phase activity and the cycle repeats itself for the duration of the sawtooth event. The observations presented give considerable support to the contention that sawtooth events are actually sequences of quasi-periodic substorms. We suggest that sawtooth events can be viewed as a magnetospheric mode similar to Steady Magnetospheric Convection intervals (SMCs) except that for sawtooth events, the flow of energy from the solar wind into the magnetosphere becomes too large to dissipate with out the periodic occurrence of substorms. We further suggest that the quasi-periodicity arises because the magnetosphere may only become susceptible to external or internal triggering after it has been driven beyond a stability threshold. This hypothesis can account for the existence of more potential external triggers (in the interplanetary magnetic field or solar wind) than teeth in that the magnetosphere may be selectively responsive to them.

1. Introduction

[2]   Although, at present, there is no precise, comprehensive phenomenological definition of what sawtooth events are, they can easily be identified in a qualitative sense. A working definition that has been adopted is that they are large-amplitude quasi-periodic oscillations of the energetic particle fluxes at geosynchronous orbit [e.g., *Belian et al.*, 1995]. These oscillations typically occur during storm intervals, they have a periodicity of approximately 2–4 hours [e.g., see, *Borovsky et al.*, 2003; *Henderson*, 2004] and are particularly prominent in the energetic proton fluxes (>50 keV). Sawtooth events occur during storms when the

ring current is enhanced and are driven by moderate to strong ($B_z \lesssim -10$ nT) and continuously southward IMF conditions. They are termed ''sawtooth events'' because the shape of the proton flux versus time traces displays a series of slow decreases followed by rapid increases that resemble the teeth of a saw blade.

[3]   The gradual flux decreases and sharp increases of each tooth are associated with strong stretching and dipolarization (respectively) of the magnetic field at geosynchronous orbit. While this behavior is strongest on the nightside, it can extend well past the terminators into the dayside, particularly on the duskside. In addition, each tooth is associated with an abrupt recovery in Sym-H [e.g., *Reeves et al.*, 2004]; [*Huang et al.*, 2004], distributed particle injections, and premidnight sector activations of the auroral distribution [e.g., *Reeves et al.*, 2004]. Although the observed phenomenology in many data sets greatly resembles that of substorms, it has been noted that the auroral activity rapidly engages a wider than usual azimuthal range and that the injections can also be dispersionless over a much wider than usual range of local times. This has led to an ongoing

---

[1]Los Alamos National Laboratory, Los Alamos, New Mexico, USA.
[2]University of California, Berkeley, Berkeley, California, USA.
[3]Johns Hopkins University Applied Physics Laboratory, Laurel, Maryland, USA.
[4]NOAA Space Environment Center, Boulder, Colorado, USA.

debate as to whether sawtooth events are (1) a series of large storm-time substorms or (2) a previously unknown (non-substorm) storm-time phenomenon that is driven by relatively rare solar wind/IMF conditions (e.g., see discussion by *Borovsky et al.* [2003]).

[4] To address this issue, *Henderson* [2004] recently reexamined the CDAW-9C interval which spanned the time period from 0000 to 1200 UT on 3 May 1986. This interval occurred during the PROMIS (Polar Region and Outer Magnetosphere) campaign when the tail region was particularly well-covered by a number of different spacecraft (AMPTE/IRM, AMPTE/CCE, ISEE-1/2, SCATHA, GOES-5/6, and three LANL geosynchronous spacecraft) and the auroral distribution was being monitored by the DE-1 and Viking spacecraft [*Pulkkinen et al.*, 1991; *Baker et al.*, 1993; *Minenko et al.*, 2000; *Hones et al.*, 1987]. Although only a single substorm was selected for analysis by the CDAW-9 community, *Henderson* [2004] found that the full extended interval was actually a sawtooth event and that the 0111 UT substorm selected for study (at CDAW-9) was an individual embedded tooth. It was conclusively demonstrated therefore that the individual teeth that comprise a sawtooth event have indeed been identified as substorms in the past.

[5] The excellent radial coverage in the tail during the CDAW-9C interval also allowed *Henderson* [2004] to show that strong tail-like stretching can extend well inside of geosynchronous orbit and that substorm-associated tail reconnection may occur inside of -11 R_E down tail. The author concludes that a major difference between sawtooth and nonsawtooth substorms is that during sawtooth events the activity in the tail is brought much closer to Earth and is maintained there for extended periods of time.

[6] Other studies of sawtooth events have focused on solar wind triggering or driving of the teeth [*Huang et al.*, 2003b; *Lee et al.*, 2004] and on the behavior of the tail field [*Huang*, 2002; *Huang et al.*, 2003a; *Lui et al.*, 2004]. *Reeves et al.* [2004], *Huang* [2002], *Huang et al.* [2003a], and *Henderson* [2004] all conclude that sawtooth events are sequences of quasi-periodic substorms, while *Lee et al.* [2004] concludes that they are not but are rather directly driven by solar wind pressure enhancements.

[7] In this paper we further examine the 18 April 2002 sawtooth event which was one of the most prominent and long-lived events of its type in the LANL geosynchronous data set. In addition, it occurred at a time when data was being acquired by six LANL-instrumented spacecraft and two NOAA GOES spacecraft. Data from these eight geosynchronous spacecraft provide an opportunity to explore the global characteristics of a sawtooth event with unprecedented coverage at geosynchronous orbit. In addition, the development of the auroral distribution during this event was captured with good spatial and temporal evolution with the IMAGE/FUV imager. Our main goals here are to (1) examine in detail the nature of the flux increases and field dipolarizations around the globe, (2) characterize in detail the global evolution and morphology of the auroral distribution, and (3) examine evidence for triggering of the individual teeth.

2. Observations

[8] In Figure 1a we show the LANL/SOPA geosynchronous energetic electron and proton measurements at six

locations around the Earth together with the field inclination angle at GOES-8 (purple) and GOES-10 (green). The flux profiles, particularly in the proton data, display the characteristic sawtooth pattern with a quasi-periodicity in the 2–4 hour range. The vertical dashed lines indicate the onset of each tooth as determined from a combination of the electron and proton measurements. Note that for the teeth near 0800 and 1120 UT, more than one dashed line is shown. In these cases, there were multiple sudden increases observed at one or more of the spacecraft.

[9] The magnetic field inclination angle at the GOES-8 and GOES-10 spacecraft are shown in the bottom panel in each of the electron and proton plots shown in Figure 1a (this data was also presented recently by *Lee et al.* [2004]). Specifically, the quantity plotted is the angle between the magnetic field vector and the Geocentric Solar Magnetospheric (GSM) equatorial plane (i.e., the $x - y$ axis). Thus an angle of 90° indicates that the field direction is perpendicular to the GSM equatorial plane (i.e., dipole-like), while low angles indicate a more tail-like stretched configuration. Differences in the behavior and magnitude of the variations between the two GOES spacecraft can be attributed to the fact that they are at different magnetic latitudes and at different local times. From Figure 1a, we can immediately see that large dipolarizations of the field at geosynchronous orbit occurred in association with the onset of some of the teeth. The 0239, 0530, 0806 UT teeth show particularly dramatic dipolarizations at GOES-10. On the other hand, we note that a relatively weaker response was observed for the 1120 UT tooth and no clear dipolarization signature at all was observed for any of the other teeth. Thus for this event, the large prominent dipolarizations seen at the GOES spacecraft were limited to times when those spacecraft were (approximately) on the nightside. This is consistent with other sawtooth events we have examined and clearly illustrates that, while abrupt flux increases are observed around the globe, the geosynchronous magnetic field dipolarization response is not global but rather typically confined (approximately) to the nightside.

[10] The behavior of the geosynhcronous magnetic field shown here is quite typical of sawtooth events in general. Other studies showing similar events have been published by *Reeves et al.* [2004], *Huang et al.* [2003b], *Henderson* [2004], and *Lee and Lyons* [2004].

[11] Note that due to the 2–4 hour periodicity of sawtooth events, the dramatic coherent oscillatory behavior is most prominently seen in full-day summary plots like those shown in Figure 1a. Also note that in these plots the individual teeth appear to represent simultaneous dispersionless flux increases at all locations around the globe. To illustrate that this is in fact not the case, we show, in Figure 1b, the LANL/SOPA energetic electron and proton particle fluxes for a 2 hour interval encompassing the 0530 UT tooth. The vertical dashed line is drawn at 0530 UT and the magnetic local time of each spacecraft is indicated. The proton data show that the flux increases observed on the dayside were clearly dispersed and that the dispersion increases as one moves west from the 1991-080 spacecraft (at dusk), through local magnetic noon to the LANL-01A spacecraft (at dawn). In addition, the only increase in the energetic electron fluxes at 0530 UT was seen at 1991-080, which was the only satellite in the dusk-to-midnight sector
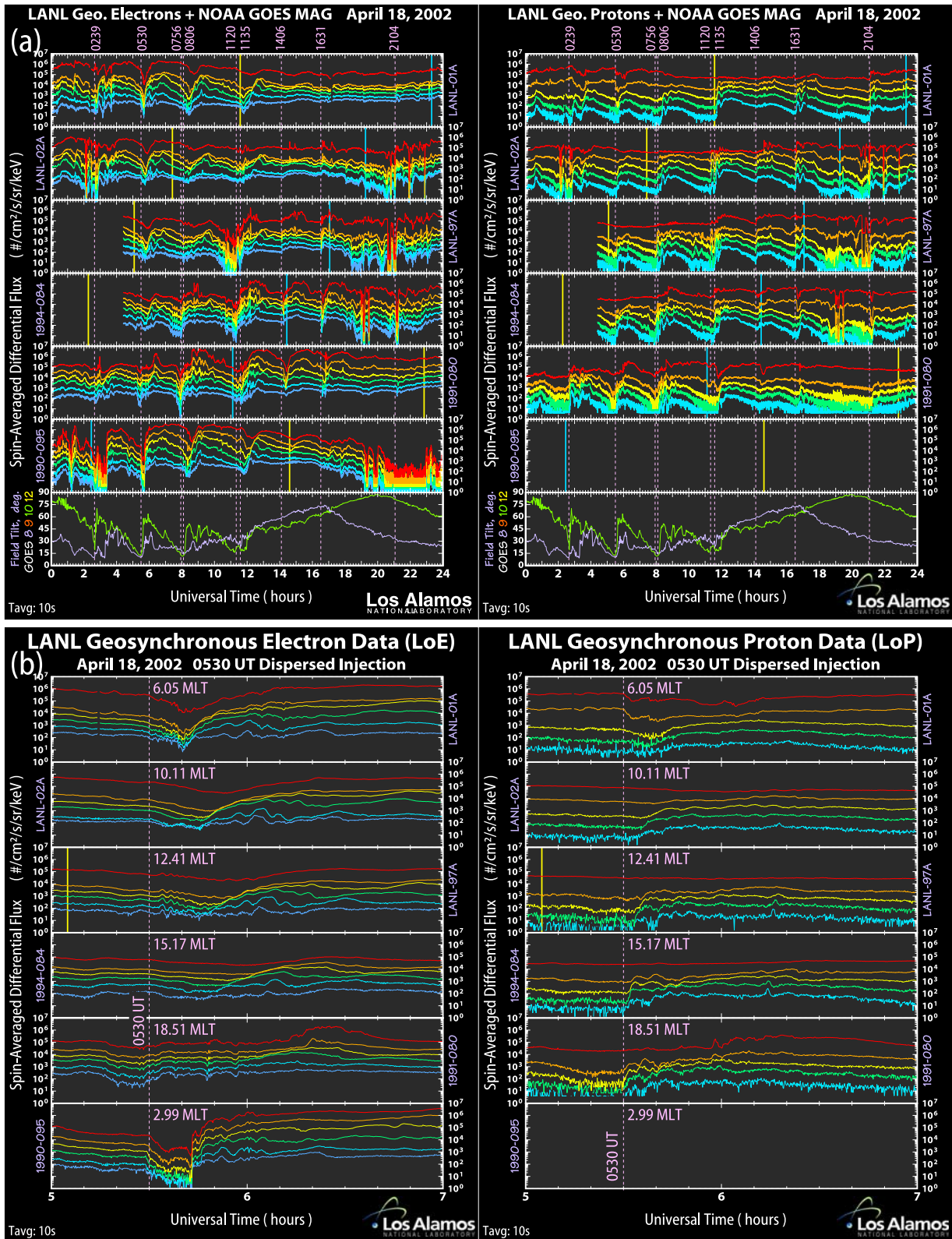
Figure 1. Los Alamos National Laboratory (LANL) energetic electron and proton data from six geosynchronous spacecraft stationed at various locations around the world together with field inclination angle at the GOES-8 and GOES-10 geosynchronous spacecraft. From red to blue, the energies shown are 50–75 keV, 75–105 keV, 105–150 keV, 150–225 keV, 225–315 keV, 315–500 keV (for electrons) and 50–75 keV, 75–113 keV, 113–170 keV, 170–250 keV, 250–400 keV (for protons). The vertical yellow and blue lines mark the time at which each satellite passed through local magnetic noon and midnight, respectively.
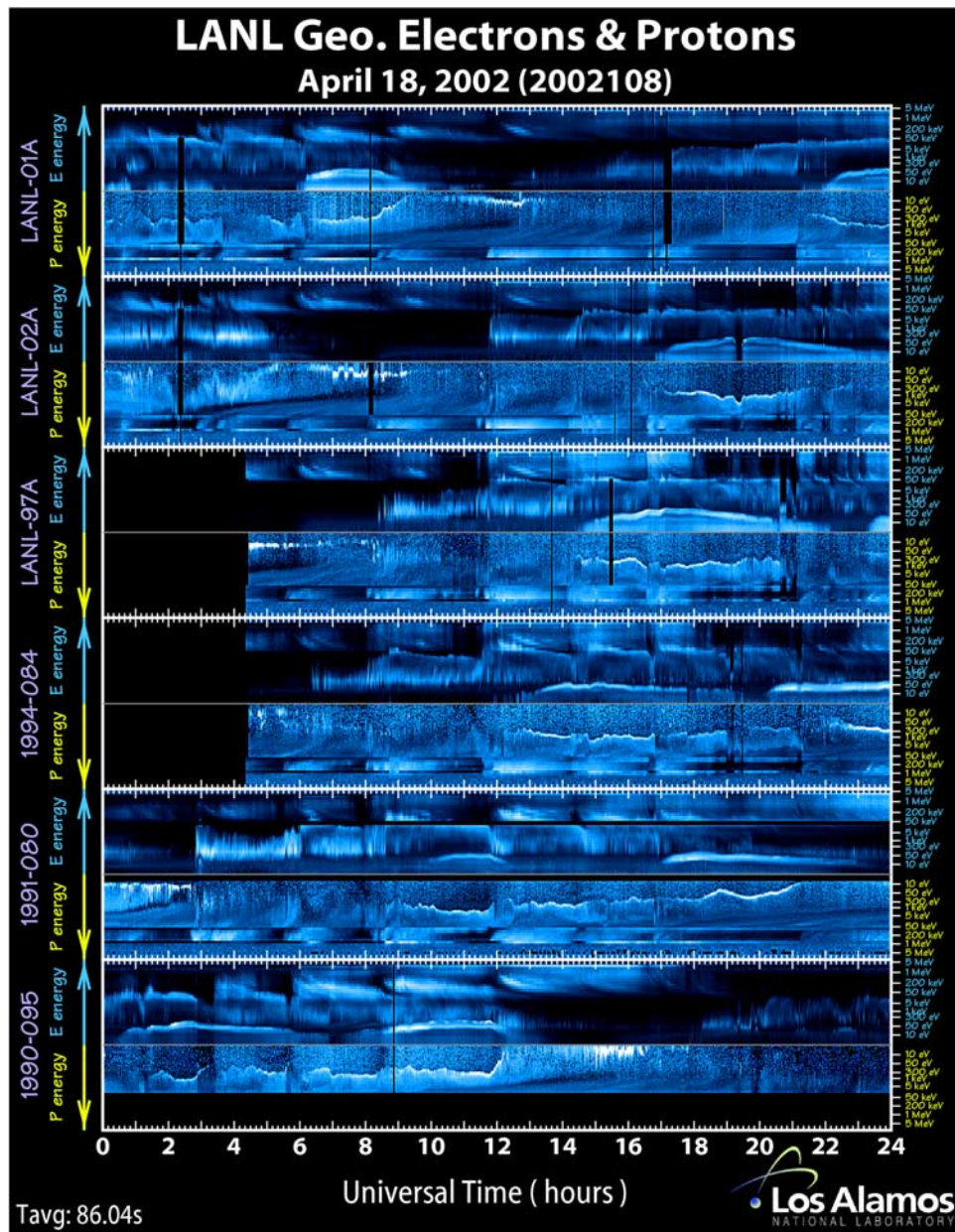
Figure 2. Los Alamos National Laboratory (LANL) energetic proton data from six geosynchronous spacecraft stationed at various locations around the world.

at that time. None of the other LANL spacecraft observed an abrupt dispersionless energetic electron increase at 0530 UT. In fact 1990-095 (in postmidnight sector) shows exactly the opposite, an abrupt flux decrease. This is followed several minutes later by a large dispersionless flux increase at around 0542 UT. In addition, all of the spacecraft show the highly dispersed signatures of drift echoes in the electron data. These observations are consistent with a fairly wide but still localized (i.e., not global) duskward skewed nightside injection region (i.e., dusk-to-midnight sector). The delayed dispersionless electron flux increases at 1990-095 in the postmidnight sector may have been due to an eastward propagation of the envelope of activity.

[12] To further illustrate the dispersive nature of the flux increases for the other teeth, we present energy versus time spectrograms for each of the LANL spacecraft in Figure 2. Data from all three LANL instruments (MPA, SOPA, ESP) are shown together in a format in which the electron energies increase up the page while the proton energies increase down the page (i.e., the so-called "McIllwain format"). The energies cover a huge range from a few eV up to several MeV. A feature of this format is that the very lowest-energy particles ($\approx$"zero" energy particles) are plotted adjacent to each other which is useful because zero-energy particles have the same drift trajectories regardless of their species. It is important to note also that the color levels in Figure 2 do not represent flux values. Since the dynamic range in fluxes is very large (several orders of magnitude), color spectrograms of flux or even energy flux are not suitable for the merged LANL data sets. Thus
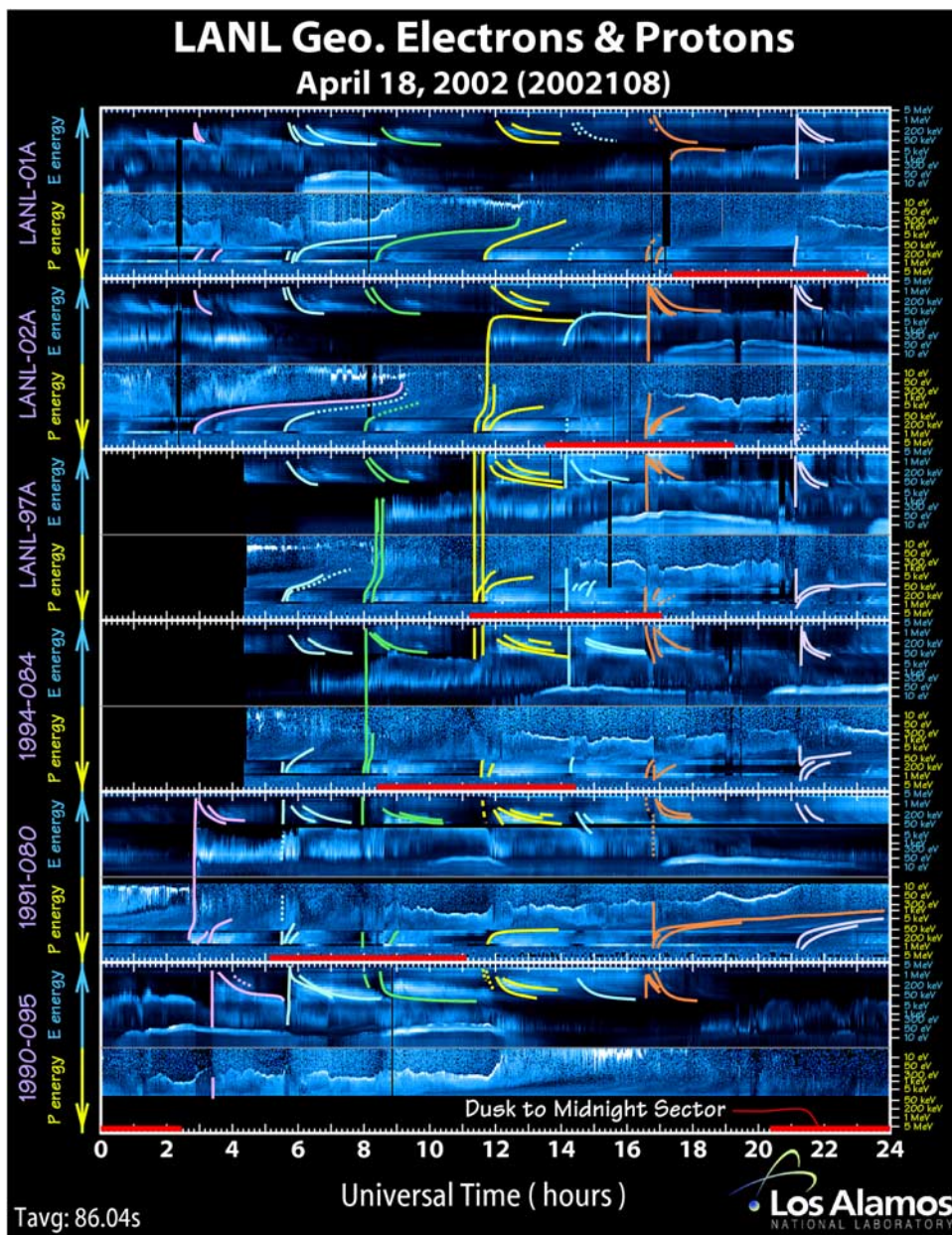
Figure 3. Annotated version of Figure 2. Various dispersion features have been (qualitatively) highlighted and the times for which each spacecraft was located within the dusk-to-midnight sector are indicated with red bars. Dispersion features associated with each tooth are grouped according to color. Dotted lines represent faint or hard to follow dispersion features. Note that type-1 dispersion patterns tend to be observed when a spacecraft is situated on the nightside.

instead of flux, color in Figure 2 represents the deviation of the flux from an average (energy-dependent) background level. These "flux perturbation maps" are very useful for identifying dispersion patterns in the data.

[13] As an interpretive aid, we present an annotated version of Figure 2 in Figure 3. We have attempted to outline (in a qualitative manner) some of the most relevant dispersion features observed. A color-coding scheme has been used in order to group the dispersion features associated with each tooth. Comparing these dispersion patterns with those expected from the *Mauk and Meng* [1983] injection boundary model (see their Figure 8), we can see that they are all either "type-1," "type-2," or "type-7"

dispersion patterns (see *Mauk and Meng*'s [1983] Figures 10, 11, and 16 for other examples of these patterns). The dominant presence of these types of dispersion patterns indicates that the injection boundary was pushed inside of geosynchronous orbit on the nightside for all of these events. We will discuss this in more detail later, but for now we wish to establish that the patterns were organized as one would expected from the *Mauk and Meng* [1983] model, both in a statistical manner and in an instantaneous manner.

[14] Statistically, we can see that for each tooth, each spacecraft observed type-2 dispersion patterns when they were near the noon-to-dusk sector, type-1 dispersion pat-
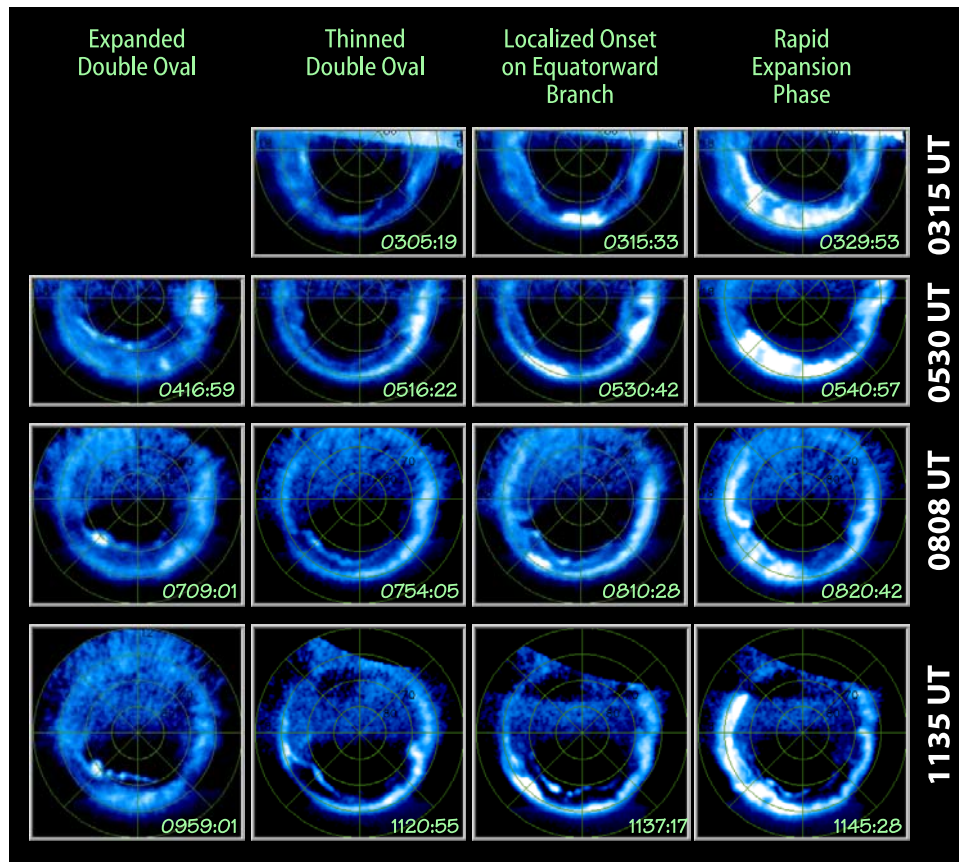
Figure 4. Selected IMAGE/FUV WIC images illustrating the behavior of the auroral distribution around the time of the onset of each tooth.

terns when they were closer to the dusk-to-midnight sectors and type-7 dispersion patterns when they were substantially eastward of the midnight region. In addition, if one focuses on a single tooth, the instantaneous distribution of dispersion patterns also agrees with this ordering. The observed dispersion patterns at geosynchronous orbit are therefore consistent with what one would expect from the standard Kp-dependent injection boundary model. They are not consistent with globally dispersionless injections but rather with ones that were more localized (but still likely quite wide in azimuthal extent) on the nightside.

[15] In Figure 4 we show selected IMAGE/FUV WIC images illustrating the behavior of the northern auroral distribution before, during, and after the onset of the 0315, 0530, 0806, and 1130 UT teeth. Each image is shown in Apex Magnetic Coordinates with noon at the top and midnight at the bottom, and we have reduced the airglow signal in order to more clearly see the entire global distribution (see *Immel et al.* [2000] for details on the airglow removal technique). The latitude circles are drawn every 10° between 50° and 90°. We have divided the figure into four columns. The third column shows the auroral distribution at (or some minutes after) the onset of each tooth while the other columns show times before (first and second columns) and after (fourth column) the onset. In all cases shown, the onset of the tooth is associated with a localized brightening of the auroral distribution in the dusk to midnight sector on the lower branch of a so-called "double oval" configuration. A double oval configuration is one in which a broadly extended (in azimuth) region of auroral emissions resides poleward of the main auroral oval. Such double oval configurations are known to develop out of the recovery phase of some substorms and are also characteristic of Steady Magnetospheric Convection (SMC) intervals.

[16] From Figure 4 we can see that the auroral distribution develops in a systematic way prior to each onset. In each case a relatively wide double oval configuration is observed on the order of an hour prior to onset (first column). This double oval progressively thins (second column) until a localized onset occurs on the equatormost portion in the dusk to midnight sector (third column). Following this, the initial brightening expands very rapidly poleward and azimuthally (fourth column). This expansion phase activity eventually evolves into the double oval type morphology (e.g., first column) and the cycle repeats itself for the duration of the sawtooth event. We note that each of these onsets looks very much like storm-time "embedded" substorm onsets and are also fully consistent with the Akasofu description of breakup occurring on the equatorwardmost arc. Embedded onsets were first discovered in the 1990s using the Viking UVI database [*Murphree et al.*, 1991; *Murphree and Cogger*, 1992; *Murphree et al.*, 1993] and typically consist of a localized premidnight sector onset on the equatorward branch of a preexisting double-oval configuration.
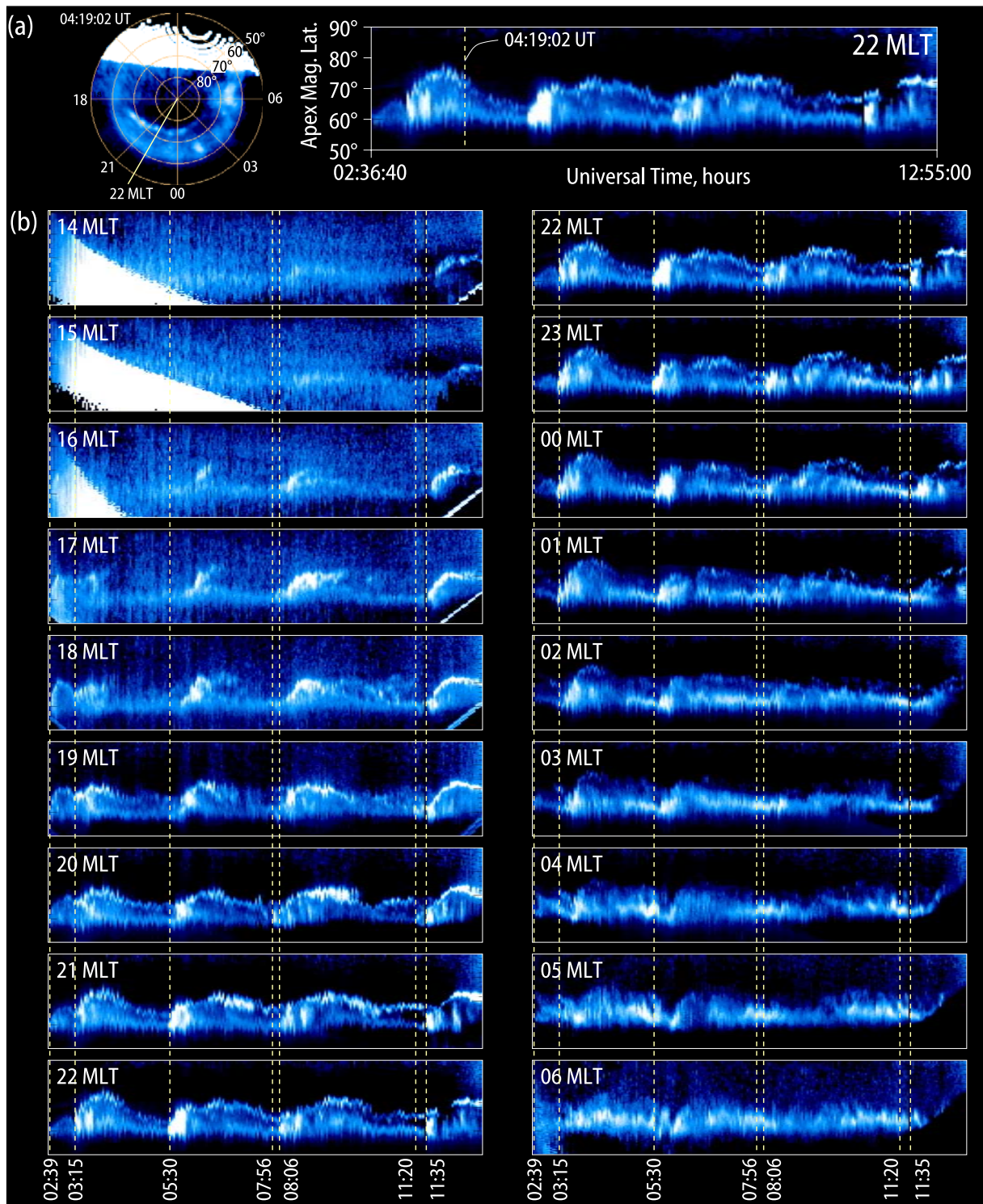
Figure 5. Keograms generated from a series IMAGE/FUV WIC images showing the latitudinal motion of the aurora. (a) An example showing how keograms are created. The auroral intensities along the a given meridian is extracted from each image and stacked next to one another to create a latitude-versus-time plot. (b) Keograms for MLT meridians ranging from 1400 MLT through midnight to 0600 MLT.

[17] Another way to view the development of the auroral distribution is shown in Figure 5. Here we present a sequence of keograms (constructed from the raw IMAGE/FUV WIC images) showing meridional slices of the auroral intensity at 17 different magnetic local times. These latitude versus time plots clearly illustrate the behavior described above. Specifically, each onset occurs on the lower branch of a thinned down double oval configuration. The aurora expands poleward and then develops into a new double oval configuration which then thins down again prior to the next

onset. From an examination of the keograms at different magnetic local times, it is also clear that the auroral distribution does not expand poleward simultaneously at all local times. The 0530 UT event, for example, clearly shows a time delay for the initial localized disturbance to propagate to the terminators. As noted above, this behavior is essentially the same as is observed for substorms, although here the onsets are "embedded" in a preexisting double oval configuration and the expansion phase is more rapid and extensive than typical isolated substorms. For the other teeth shown in Figure 5, the azimuthal expansion is more simultaneous (but still with some delay) in the dusk to midnight sector, but we note that the expansion into the morning sector is still significantly delayed and there is often little or no signature beyond 0300–0400 MLT.

[18] The data presented in Figures 4 and 5 clearly show that the explosive auroral disturbances associated with each tooth are not simultaneously global phenomena, but rather they begin in a fairly localized region in the dusk to midnight sector and expand rapidly in the azimuthal and poleward directions. Nevertheless, one may note that dynamic auroral activity still occurs over a wider azimuthal expanse throughout the sawtooth event. For example, a number of auroral streamer events are observed which begin at the poleward branch of the double oval configuration and propagate equatorward. In the keograms of Figure 5 these can be seen as equatorward moving lines. In addition, for most of the sawtooth event, the auroral oval in the midnight to postdawn sector is quite active and displays eastward propagating omega-band forms. As shown by *Henderson et al.* [2002], auroral streamers can evolve into torch-like structures and omega bands during active times and, although omega bands are commonly associated with substorm recovery phase, they can also occur during SMCs. In general, omega bands tend to be associated with the dynamics of the double oval configuration whether such a configuration is produced as a remnant of a prior substorm onset (i.e., a recovery phase feature) or is a more long-lived configuration typical of SMC events. For the 18 April 2002 sawtooth event, both the double oval configuration and intense eastward propagating omega-band forms are prominent features that exist in the auroral distribution throughout the event in addition to the quasi-periodic substorm-like onsets. This is typical of sawtooth events and illustrates that sawtooth events behave very much like SMCs that are punctuated in a quasi-periodic manner by (embedded) substorms.

[19] An interesting and important aspect of sawtooth events is that they tend to be driven by solar wind/IMF conditions that are very similar to those that drive SMCs. Specifically, both types of events tend to develop when the IMF is continuously southward and reasonably steady for prolonged periods of time. Thus an interesting question that arises is, For steady southward IMF driving conditions, what controls whether the magnetospheric response is an SMC or a sawtooth event? One clue to this as yet unresolved issue is that sawtooth events tend to occur when the IMF Bz is moderately to strongly negative while SMCs tend to develop when the IMF Bz is weakly to moderately negative. Although notable exceptions to this ordering have been identified [e.g., *Zhou et al.*, 2003] and other factors like polar cap potential saturation [*Siscoe et al.*, 2002;
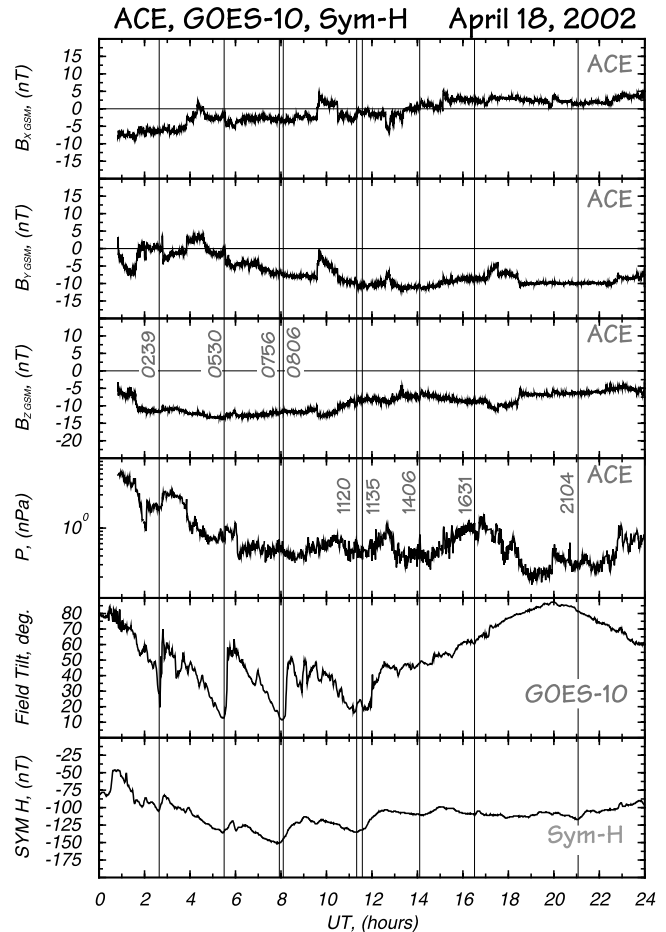

Figure 6. Interplanetary magnetic field and solar wind data from the ACE spacecraft together with the GOES-10 field inclination angle and the Sym-H index.

Siscoe et al., 2004], solar wind Mach number [*Borovsky*, 2004], and ionospheric conductance and bowshock standoff distance [*Merkine et al.*, 2003] effects may be important contributors to the overall efficiency of the solar wind-magnetosphere coupling, on average sawtooth events appear to be more strongly driven than SMCs are. Therefore sawtooth substorms may result because the magnetosphere may not be able to dissipate the energy input in a relatively steady-state manner like it manages to during SMCs. We therefore propose that sawtooth events are a manifestation of the magnetosphere's need to globally "reset" or "reconfigure" itself via substorms in a quasi-periodic manner when it is strongly driven. This naturally leads us to a number of additional questions: (1) Are the substorms spontaneous or are they triggered? (2) What controls the quasi-periodicity?

[20] In order to explore these questions, we show IMF and solar wind data from the ACE spacecraft in Figure 6. The IMF B_x, B_y, and B_z components are shown in the upper three panels. The solar wind dynamic pressure (on a log scale) is shown in the fourth panel and the GOES-10 field inclination angle and Sym-H index are shown in the bottom two panels. The ACE data have been appropriately time-shifted and the times of the individual teeth are indicated with solid vertical lines. It is apparent from the ACE data
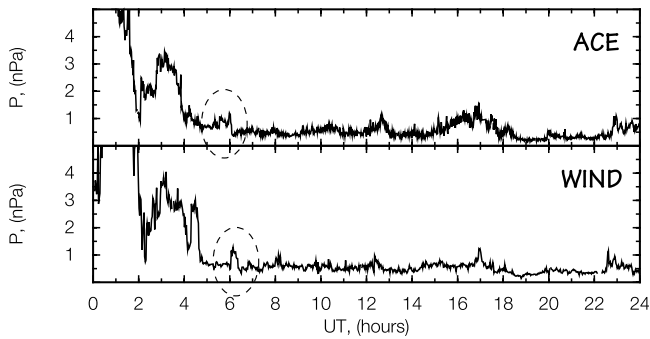
**Figure 7.** Solar wind dynamic pressure variations seen at ACE and Wind.

that there are a number of abrupt changes in the IMF in addition to a number of small to moderate sized fluctuations in the dynamic pressure. Nevertheless, it is difficult to see a clear one-to-one correspondence between these disturbances and the sawteeth. Although one could perhaps associate a pressure enhancement with the onset of each tooth (as was done by *Lee et al.* [2004]), there appears to be many more fluctuations in the IMF/SW than there are teeth. Finally, there appears to be neither an obvious 2–4 hour periodicity to the IMF/SW disturbances nor an obvious sawtooth waveform in the the pressure profile. Nevertheless, we did find compelling evidence that at least one of the teeth could have been triggered by a solar wind pressure pulse.

[21] In Figure 8 we present a subset of the data shown in Figure 6 together with magnetic field data from the Polar spacecraft. The ACE, GOES-10, and Sym-H data are plotted for the time interval between 0200 and 1000 UT, while the Polar magnetic field data are shown for times between 0400 and 0700 UT, which spans the onset of the 0530 UT tooth. At 0530 UT, Polar was near the SM equatorial plane in the prenoon dayside sector between geosynchronous orbit and the magnetopause. Note that just prior to the 0530 UT onset, Polar observed an abrupt change in both the field direction and strength. This behavior is consistent with the sudden entry of Polar into the magnetosheath caused by the impact of a pressure pulse. If we examine the dynamic pressure in Figures 6 and 8, we can see a (surprisingly) weak disturbance near 0530 UT. Thus it is quite possible that the pressure pulse that caused the excursion of Polar into the sheath was not well observed by ACE in its halo orbit around the L1 point, a point that has been made in previous substorm triggering studies [e.g., *Lyons et al.*, 1997; *Blanchard et al.*, 2000].

[22] In order to examine this hypothesis in more detail, in Figure 7 we compare the solar wind dynamic pressure seen at ACE with that seen at the Wind spacecraft which was situated very far off the Earth-Sun line in the $+Y_{GSM}$ direction at $R_{GSM} = (10.9, 191.7, 75.1)$ R_E. In this figure, the ACE data is still time-shifted, but we have not applied any time shift to the Wind data because it is so close to the $X_{GSM} = 0$ axis to begin with. Note that the gross features seen at ACE and Wind are similar but, as expected, significant differences in structure and timing exist between the two spacecraft. Clearly, the distribution of the pressure in the solar wind varies temporally, spatially or both. Nevertheless, the Wind data do show a much more prom-

inent pressure pulse in the 0600–0630 UT time frame. Given the large off-axis distance of Wind and the fact that SW discontinuities are often oblique relative to the Earth-Sun line, the pressure pulse in the Wind data could certainly have been the same one that we associate with the Polar sheath excursion prior to the 0530 event.

[23] Finally, in Figure 9 we introduce IMAGE/MENA and IMAGE/HENA energetic neutral atom (ENA) imager data during the sawtooth event together with composition data from the Polar/CAMMICE MICS instrument. Also shown are the ACE Bz and dynamic pressure curves, proton fluxes from two of the LANL detectors, and the GOES-10 field inclination angle and the Sym-H index. The HENA and MENA data are shown in more condensed angle versus time plots rather than images. The MENA data shows (polar angle summed) ENA flux as a function of spin phase and time, while the HENA panels show (spin phase summed) ENA flux as a function of polar angle and time. In these formats the gross temporal development of the ENA fluxes can more easily be monitored as a function of time. We note from the HENA hydrogen panel that each tooth was associated with a stepwise increase in the ENA emission rate which indicates that each tooth was associated with an injection of energetic protons into the ring current. The
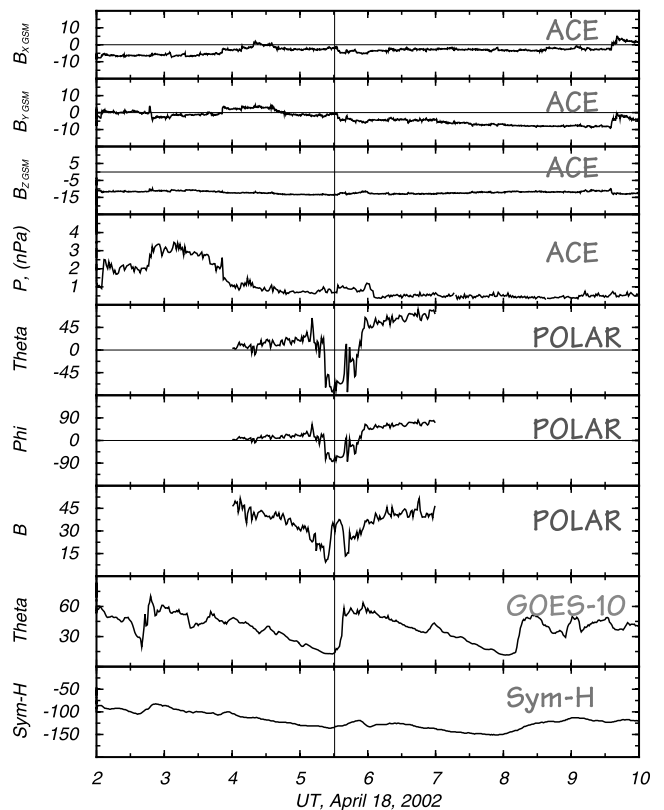
Figure 8. Interplanetary magnetic field and solar wind data from the ACE spacecraft together with Sym-H index and magnetic field measurements at Polar. During the onset of the 0530 UT event, Polar was situated in the dayside prenoon sector. Just prior to the onset, Polar suddenly entered the sheath suggesting that the magnetosphere was dynamically compressed by a pressure pulse just prior to the onset of the substorm.
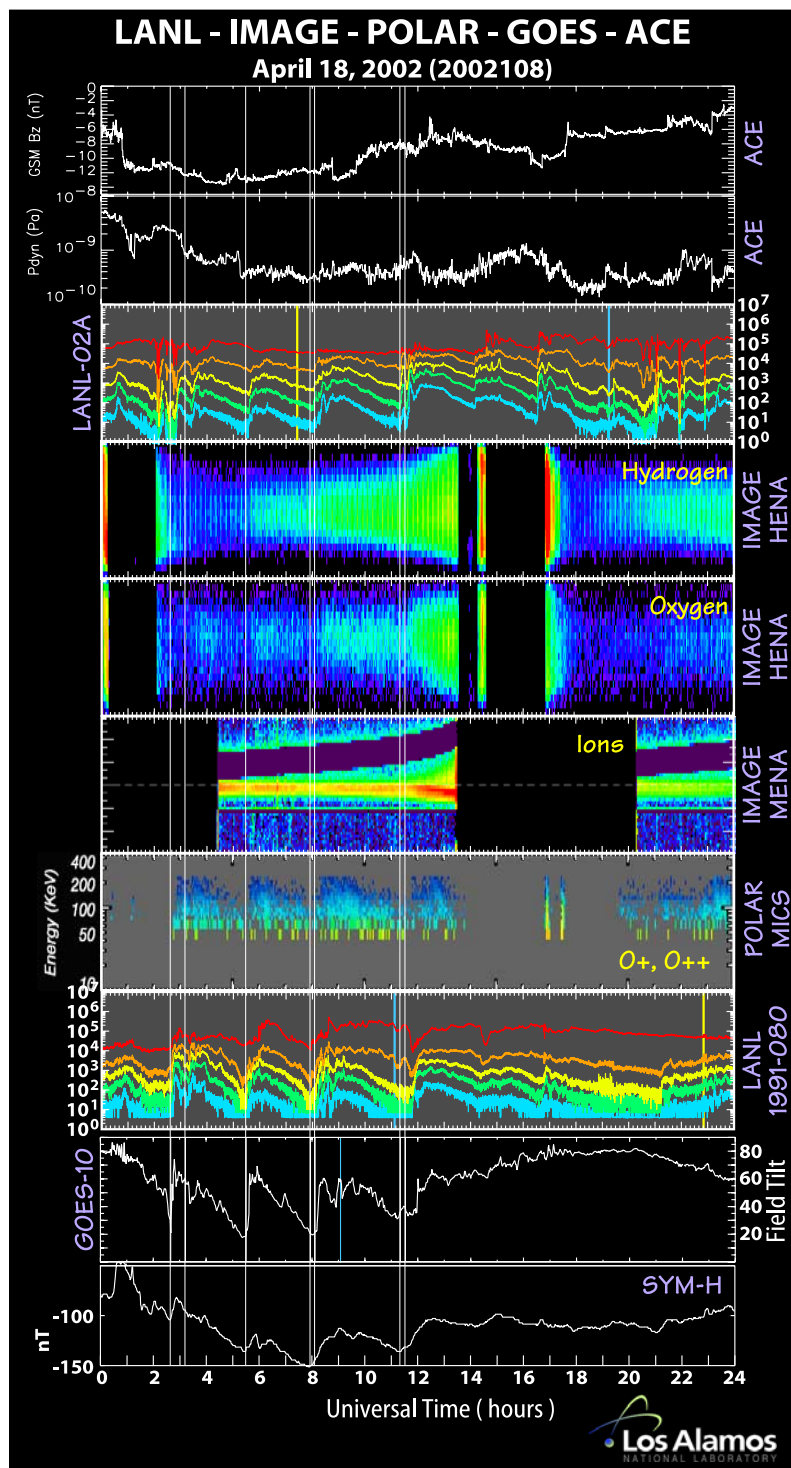
Figure 9. IMAGE/MENA and IMAGE/HENA energetic neutral atom data together with ion composition data from Polar/MICS; field inclination angle at GOES-10, Sym-H, ACE *Bz* and dynamic pressure and protons fluxes from two of the LANL geodetectors.

lower-energy MENA measurements also show a modulation in ENA fluxes associated with the individual teeth, but the fluxes do not always increase in a stepwise manner. The HENA oxygen [*Mitchell et al.*, 2003] panel shows that each tooth was also associated with bursts of oxygen ENAs. This is consistent with the in situ measurements of low charge state oxygen ions (of ionospheric

origin) made with the MICS instrument. From the HENA and MICS observations it is clear that sawtooth events are associated with the injection of oxygen-rich energetic particles into the ring current.

[24] IMAGE/HENA hydrogen (19–60 keV) and oxygen (52–222 keV) ENA images acquired before, during and after the 1135 UT onset are presented in Figure 10. A
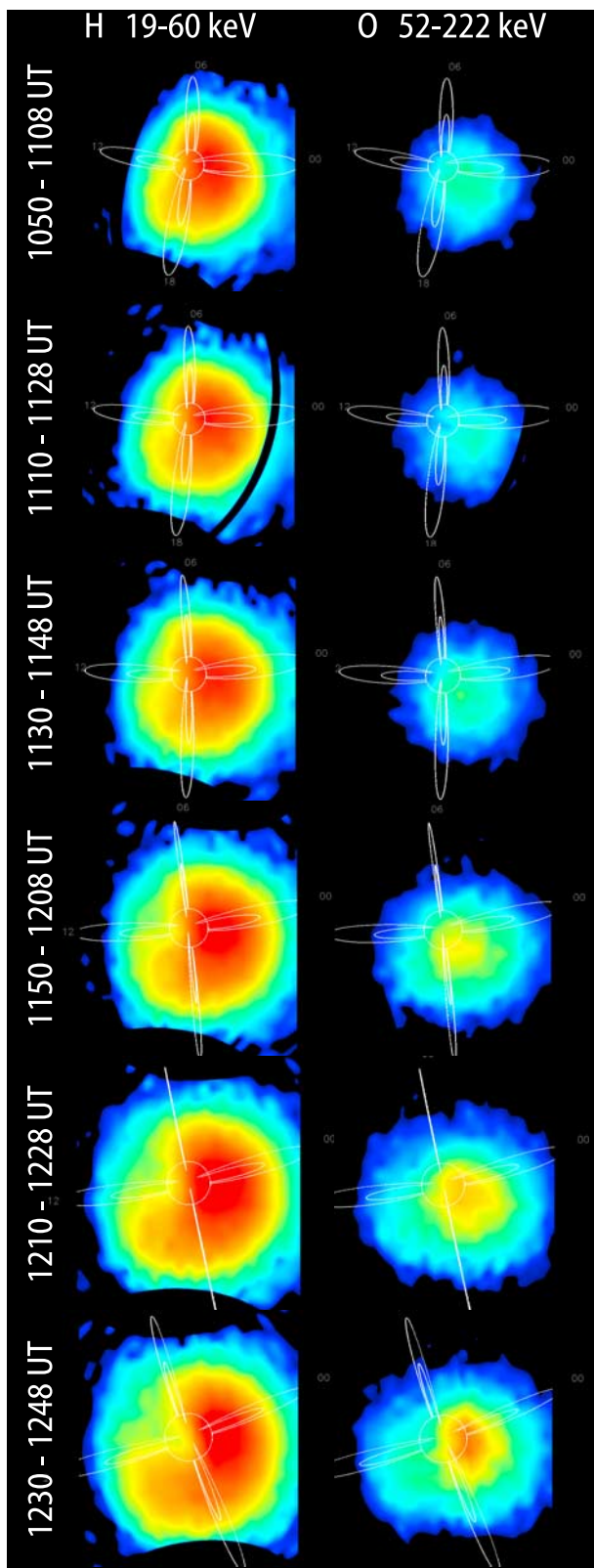
Figure 10. IMAGE/HENA ENA images spanning the time of onset of the 1135 UT tooth. The view is from the northern hemisphere with local magnetic noon to the left and local magnetic midnight to the right. Note the westward propagating injection on the duskside (bottom of each image) from the nightside to the noon meridian in the hydrogen images between the third and sixth frames.

notable feature of the H images is that the nightside is continuously intensified throughout the sequence, but following onset, the emissions can be seen expanding westward from the nightside to the noon meridian. This behavior is entirely consistent with that observed in a previous Polar ENA superposed epoch study of storm-time injections [*Reeves and Henderson*, 2001]. Furthermore, the sequence of images shown in Figure 10 visually confirms our earlier conclusion that the onset of the teeth are not globally dispersionless but rather propagate away from the nightside. The oxygen images shown in the right hand column also indicate that oxygen emissions during this onset were enhanced in the dusk to midnight sector. (Note that due to scattering in the HENA entrance aperture foil, oxygen is not well resolved spatially and localized features will therefore appear to be considerably blurred.)

3. Discussion and Conclusions

[25] In our analysis of the 18 April 2002 storm-time sawtooth interval, we have shown that the strong dipolarization signatures observed at geosynchronous orbit are confined to the nightside and that there is therefore not a globally simultaneous response for each tooth. We have also shown that the injection signatures are not globally dispersionless for each tooth. In fact there is significant dispersion associated with each flux increase and this dispersion is consistent with an unusually wide (in azimuth) substorm injection region centered approximately in the dusk to midnight sector. It is interesting to note that such wide injection regions at geosynchronous orbit can easily be achieved in the empirical *Kp*-dependent injection boundary model. As discussed by *Singer et al.* [1983], the inner edge of the plasma sheet lies inside of geosynchronous orbit for high values of the *Kp* index and as shown by *Mauk and McIlwain* [1974] and *Mauk and Meng* [1983], the injection boundary is pushed entirely inside of geosynchronous orbit on the nightside for *Kp* levels as low as 5. Such *Kp* levels are consistent with geomagnetic storm conditions in general and with the 18 April 2002 event in particular (*Kp* levels for the day were: $7_\circ$, 7_-, 6_-, 6_-, 4_+, 5_-, $4_\circ$, 4_+).

[26] In order to demonstrate that the dispersion patterns observed in Figures 2 and 3 are consistent with the standard injection boundary picture, we simulated the dispersion patterns expected at the six LANL geosynchronous spacecraft for the 1135 UT onset using the *Mauk and Meng* [1983] *Kp*-dependent injection boundary model. We used a simple centered dipole field and a *Kp*-dependent, shielded Volland-Stern electric field to trace electrons and protons backward in time (to the onset time of 1135 UT) from each spacecraft. For the simulation, we restricted the azimuthal definition of the injection boundary to be between 1800 and 2400 MLT (i.e., we assume the dispersionless injection occurred in the dusk to midnight sector), and we assumed that all of the particles were equatorially mirroring (zero second invariant). The results are presented in Figure 11a which is similar in format to the merged MPA/SOPA/ESP spectrograms shown in Figure 2. The color-coding indicates how far (radially) behind the injection boundary the particles originated, with red being closest to the boundary. If the particle originated more than 10 R_E tailward of the injection boundary, it was colored gray.
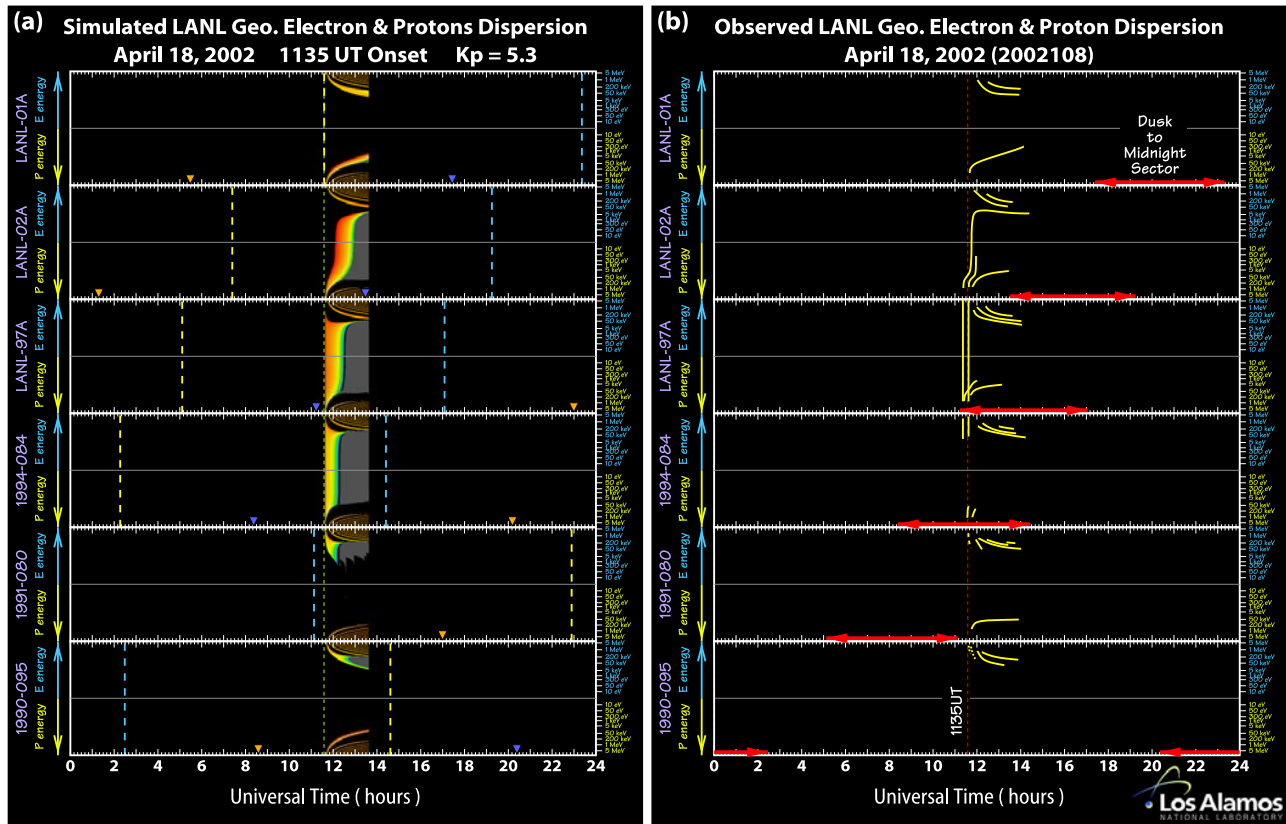
Figure 11. (a) Simulated dispersion patterns at geosynchronous orbit for the 1135 UT tooth. (b) Observed dispersion patterns for the 1135 UT tooth.

[27] It is important to note that the colored areas in Figure 11a do not represent flux levels or even flux perturbation levels (as in Figures 2 and 3). Instead, they indicate whether or not particles of a given species and energy, originating from behind an injection boundary (between dusk and midnight), had access to a given spacecraft at a given time. In essence they represent energy- and species-dependent arrival time "curves" for each spacecraft. The multivalued nature of the regions in the horizontal direction arise due to the periodic drift motion of the particles. For example, the bands of dispersed curves seen at higher energies in both the electron and proton panels represent the routinely observed injection-associated drift echoes (e.g., see Figure 9 of *Mauk and Meng* [1983]). These curves are highly idealized in Figure 11a because (1) we have only considered equatorially mirroring particles, and (2) we have not taken into account energy dispersion within the energy passbands of the LANL detectors. In reality, both of these factors will tend to smear the signals together in such a way that only the first several drift echoes can easily be separated.

[28] Because Figure 11a shows us when we should expect the injected particles to arrive at each spacecraft (given the assumed injection model), the patterns can be compared directly to those shown in Figure 3. Note that since Figures 2 and 3 show real flux perturbation levels, the arrival of obvious injection-associated flux enhancements will only be visible in the perturbation maps: (1) for energies that were actually injected, and (2) for

energies that actually experienced a net change in their flux levels relative to the background flux levels. In Figure 11b, we have reproduced the dispersion curves from Figure 3 only for the 1135 UT injection. Note that although the model we used is quite crude, the simulated results in Figure 11a are qualitatively very similar to the actual dispersion features shown in Figure 11b. This demonstrates very clearly that sawtooth-like dispersion around the globe can easily be achieved with the standard Kp-dependent injection boundary model and is consistent with an injection of particles on the nightside (although some teeth may also be associated with injections that encroach somewhat past the terminators into the dayside).

[29] In this paper we have also shown that the auroral distribution was characterized by a dynamic double oval configuration, which was observed to gradually thin down in unison with the gradual flux decreases at geosynchronous orbit. The onset of each tooth was associated with a localized explosive brightening in the dusk to midnight sector on the lower branch of the double oval, and this was followed by rapid poleward and azimuthal expansion and the gradual emergence of a new expanded double oval configuration. The cycle then repeats itself. We note also that eastward propagating omega bands were a prominent feature of the auroral distribution and that due to the cyclical nature of the event, recovery phase features from one substorm can be seen merging into the growth phase of the next. Phenomenologically, the auroral configuration

looks much like that of an SMC except that here the double oval cyclically thins and expands (i.e., polar cap area cyclically increases and contracts) and is punctuated periodically by substorm expansions. This is consistent with the simultaneous operation of both a loading-unloading (substorms) and directly driven magnetospheric response.

[30] In a recent paper, *Lee et al.* [2004] suggest that the dramatic geosynchronous energetic particle flux variations during the 18 April 2002 and other sawtooth events were not due to a sequence of quasi-periodic substorms but instead were driven directly by external pressure variations. Although they noted that "some substorm effects could simultaneously have occurred on the nightside," they further suggest that "the solar wind pressure effect was the dominant cause of the sawtooth oscillations." Note that this is a very different scenario from one in which the teeth are substorms which may or may not have been triggered by external pressure (or other types of) variations. In the *Lee et al.* [2004] scenario, the sudden increase and gradual decrease of the geosynchronous fluxes associated with each tooth is directly driven or modulated by the externally imposed pressure variations.

[31] In our analysis of the IMF/SW data from ACE and Wind, we find that the event occurred during a prolonged interval of continuously southward, moderate-strong, and reasonably steady IMF with numerous small to medium sized pressure fluctuations. However, we did not find the solar wind pressure to be modulated in a characteristic sawtooth waveform. Although many pressure enhancements can be identified (particularly on a log-scale), some were short-lived pulses occurring on increasing, decreasing, or flat trends, while others were followed by net increasing or decreasing trends. In addition, the strongest pressure enhancements were not observed in association with the largest flux enhancements. Finally, while it is impossible to know exactly what pressure profile actually impinged upon the Earth, the available data indicates that there were more pressure enhancements than there were teeth. These observations alone tend to argue against a directly driven scenario; however, this argument is considerably strengthened when one considers the magnetospheric data presented here.

[32] As we already mentioned, the onset of each tooth was associated with an embedded substorm onset on the lower branch of a thinned double-oval auroral configuration. These onsets were not global in nature but were rather localized (approximately) to the nightside. In addition, we do not find evidence that substorm onsets occurred in the absence of a geosynchronous tooth onset. In other words, during the interval of good quality auroral imaging, we find a one-to-one correlation between auroral substorm onsets and the geosynchronous energetic particle flux increases defining the start of each tooth. In addition, as we discussed above the particle dispersion observed at geosynchronous orbit is fully consistent with a large-scale injection of particles on the nightside of the Earth. Together these observations very strongly indicate that the initial sharp flux increases were associated with impulsive, dynamical substorm injection events.

[33] It is also interesting to note that sawtooth waveforms always occur in a consistent, systematic manner with large, rapid flux increases separated by intervals of gradual flux decreases. They do not occur in the reverse sense with gradual increases separated by rapid decreases. Since the solar wind dynamic pressure input during sawtooth events typically does not itself display a dramatic well-defined sawtooth waveform (e.g., none of the four events studied by *Lee et al.* [2004] have well-defined sawtooth waveforms in the dynamic pressure), we surmise that if dynamic pressure drives sawtooth events, the pressure enhancements must induce a magnetospheric response that is far more coherent than the input signal. In addition, as we have already mentioned, there are often far more enhancements in the dynamic pressure than there are teeth. From this we surmise that the response must also be nonlinear in the sense that once a tooth develops, it does not become interrupted by another tooth until it has undergone the cyclical response we have described above. These two points also argue rather strongly against a directly driven scenario but are still quite consistent with one in which a 2–4 hour magnetospheric process (e.g., a substorm) is triggered at regular intervals. This could be achieved if the magnetosphere became unstable to external or internal triggering at 2–4 hour intervals.

[34] Nevertheless, we certainly do not discount the idea that external pressure (or other) variations can modulate auroral emissions or other magnetospheric behavior. For example, a shock-induced globally dispersionless proton flux increase that occurred near the end of the 11 August 2000 sawtooth event has been presented recently by *Lee and Lyons* [2004] (see their Figure 9). In addition, there is a body of evidence emerging that suggests that under strongly driven conditions, the solar wind-magnetosphere coupling may become dramatically modified relative to weakly driven conditions. For example, *Siscoe et al.* [2002] and *Siscoe et al.* [2004] have shown that when the transpolar potential is at or near saturation, the nominal Chapman-Ferraro currents can be "usurped" by region-1 currents. In such a configuration, the solar wind dynamic pressure is held off directly by these region-1 currents which map into the ionosphere. When this happens, pressure variations could therefore be expected to directly affect the ionospheric field aligned currents (and/or conductivity). It is interesting to note that this effect could potentially be associated with (dayside?) portions of the double oval configuration that is prominently observed during strongly driven times, although the plausibility of such a connection should be explored in more detail in future work.

[35] Another suggestion that has recently been proposed is that the magnetospheric response to solar wind/IMF driving conditions may be different during sawtooth intervals because statistically, sawtooth events tend to occur when the solar wind Mach number is anomalously low which "creates an unusual magnetosheath flow with extremely low beta values" [*Borovsky*, 2004]. Such conditions would also be expected to move the bowshock sunward which would also contribute to transpolar potential saturation effects as discussed by *Merkine et al.* [2003] and *Siscoe et al.* [2004]. In addition, the jump conditions across the bowshock may become substantially more complex for weak (low Mach number) shock conditions (J. E. Borovsky, private communication, 2004). Although more work needs to be done in order to ascertain exactly how these ideas may modify the

global response, these studies certainly suggest that the global response during sawtooth events may be dramatically modified relative to less strongly driven conditions.

[36] However, despite the likelihood of anomalous solar wind magnetosphere coupling during sawtooth events and the potential for shock-induced globally dispersionless flux increases, in the present study we find extremely compelling evidence that the teeth studied here are in fact substorms. We also find strong evidence that at least one of the teeth (the 0530 UT event) was triggered by a pressure pulse which moved the magnetopause across the Polar spacecraft just prior to onset. These observations suggest that when a tooth occurs, the magnetosphere becomes unresponsive to further triggers (or internal instabilities) for a 2–3 hour sawtooth growth-phase period. We therefore propose that the periodicity of sawtooth events is determined by the time it takes the magnetosphere to be driven past some stability threshold. Individual teeth could then occur either spontaneously via some type of internal instability, or they could be triggered by external pressure or IMF variations. Under this hypothesis, the sawtooth periodicity is set by the magnetosphere because it only becomes receptive to potential triggers (or internal instabilities) during a small time window near the end of each growth phase. This idea can also explain the quasi-periodicity in the sense that a tooth could be triggered anywhere within such a time window.

[37] In conclusion, from our analysis of magnetospheric and auroral data acquired during the 18 April 2002 event we find strong support for the contention that sawtooth events are actually sequences of recurrent quasi-periodic substorms. Also we suggest that sawtooth events can be viewed as a magnetospheric mode similar to SMCs except that for sawtooth events, the flow of energy from the solar wind into the magnetosphere becomes too large to dissipate without the (literally) periodic occurrence of substorms. Stated differently, it appears that the magnetosphere is continuously "driven" toward substorm-like reconfigurations in order to "reset" itself at periodic intervals.

References

Baker, D. N., et al. (1993), CDAW-9 analysis of magnetospheric events on May 3, 1986: Event-c, *J. Geophys. Res.*, 98, 3815–3834.

Belian, R. D., T. E. Cayton, and G. D. Reeves (1995), Quasi-periodic, substorm associated, global flux variations observed at geosynchronous orbit, in *Space Plasmas: Coupling Between Small and Medium Scale Processes*, edited by M. Ashour-Abdalla, T. Chang, and P. Dusenbery, p. 143, AGU, Washington, D. C.

Blanchard, G. T., L. R. Lyons, and J. Spann (2000), Predictions of substorms following northward turnings of the interplanetary magnetic field, *J. Geophys. Res.*, 105, 375–384.

Borovsky, J. E. (2004), Global sawtooth oscillations of the magnetosphere, *EOS Trans. AGU*, 85, Fall Meet. Suppl., Abstract SM23B–04.

Borovsky, J. E., R. J. Nemzek, C. W. Smith, R. M. Skoug, and C. R. Clauer (2003), The solar-wind driving of periodic substorms and global sawtooth oscillations: What determines the periodicity?, *Rep. LAUR-03-8368*, Los Alamos Natl. Lab., Los Alamos, N. M.

Henderson, M. G. (2004), The May 2–3 1986 CDAW–9C interval: A sawtooth event, *Geophys. Res. Lett.*, 31, L11804, doi:10.1029/2004GL019941.

Henderson, M. G., L. Kepko, H. E. Spence, M. Connors, J. B. Sigwarth, L. A. Frank, H. J. Singer, and K. Yumoto (2002), The evolution of north-south aligned auroral forms into auroral torch structures: The generation of omega bands and ps6 pulsations via flow bursts, in *Proceedings of the Sixth International Conference on Substorms*, edited by R. M. Winglee, pp. 169–174, Univ. of Wash., Seattle, Wash.

Hones, E. W., C. D. Anger, J. Birn, J. S. Murphree, and L. L. Cogger (1987), A study of a magnetospheric substorm recorded by the Viking auroral imager, *Geophys. Res. Lett.*, 14, 411–414.

Huang, C. S. (2002), Evidence of periodic (2–3 hour) near-tail magnetic reconnection and plasmoid formation: Geotail observations, *Geophys. Res. Lett.*, 29(24), 2189, doi:10.1029/2002GL016162.

Huang, C. S., J. C. Foster, G. D. Reeves, G. Le, H. U. Frey, C. J. Pollock, and J. M. Jahn (2003a), Periodic magnetospheric substorms: Multiple space-based and ground-based instrumental observations, *J. Geophys. Res.*, 108(A11), 1411, doi:10.1029/2003JA009992.

Huang, C. S., G. D. Reeves, J. E. Borovsky, R. M. Skoug, Z. Y. Pu, and G. Le (2003b), Periodic magnetospheric substorms and their relationship with solar wind variations, *J. Geophys. Res.*, 108(A6), 1255, doi:10.1029/2002JA009704.

Huang, C. S., J. C. Foster, G. D. Reeves, J. L. Chau, K. Yamoto, and K. Kitamura (2004), Variations of low-latitude geomagnetic fields and dst index caused by magnetospheric substorms, *J. Geophys. Res.*, 109, A05219, doi:10.1029/2003JA010334.

Immel, T. J., J. D. Craven, and A. C. Nicholas (2000), An empirical model of the OI FUV dayglow from DE-1 images, *J. Atmos. Sol. Terr. Phys.*, 62, 47–64.

Lee, D., and L. R. Lyons (2004), Geosynchronous magnetic field response to solar wind dynamic pressure pulse, *J. Geophys. Res.*, 109, A04201, doi:10.1029/2003JA010076.

Lee, D., L. R. Lyons, and K. Yumoto (2004), Sawtooth oscillations directly driven by solar wind dynamic pressure enhancements, *J. Geophys. Res.*, 109, A04202, doi:10.1029/2003JA010246.

Lui, A. T. Y., T. Hori, S. Ohtani, Y. Zhang, X. Y. Zhou, M. G. Henderson, T. Mukai, H. Hayakawa, and S. B. Mende (2004), Magnetotail behavior during storm time "sawtooth events", *J. Geophys. Res.*, 109, A10215, doi:10.1029/2004JA010543.

Lyons, L. R., G. T. Blanchard, J. C. Samson, R. P. Lepping, T. Yamamoto, and T. Moretto (1997), Coordinated observations demonstrating external substorm triggering, *J. Geophys. Res.*, 102, 27,039–27,051.

Mauk, B. H., and C. E. McIlwain (1974), Correlation of Kp with the substorm-injected plasma boundary, *J. Geophys. Res.*, 79, 3193–3196.

Mauk, B. H., and C. I. Meng (1983), Characterization of geostationary particle signatures based on the "injection boundary" model, *J. Geophys. Res.*, 86, 3055–3071.

Merkine, V. G., K. Papadopoulos, G. Milikh, A. S. Sharma, X. Shao, J. Lyon, and C. Goodrich (2003), Effects of the solar wind electric field and ionospheric conductance on the cross polar cap potential: Results of global mhd modeling, *Geophys. Res. Lett.*, 30(23), 2180, doi:10.1029/2003GL017903.

Minenko, L. V., P. A. Sedykh, and V. M. Mishin (2000), The chain of recurrent substorms on May 3, 1986, and magnetotail length fluctuations, in *Proceedings of the Fifth International Conference on Substorms*, edited by A. Wilson, pp. 59–62, Eur. Space Agency, Paris.

Mitchell, D. G., P. C. Brandt, E. C. Roelof, D. C. Hamilton, K. C. Retterer, and S. Mende (2003), Global imaging of O$^+$ from IMAGE/HENA, *Space Sci. Rev.*, 109, 63–75.

Murphree, J. S., and L. L. Cogger (1992), Observations of substorm onset, in *Proceedings of the First International Conference on Substorms*, ESA SP-335, pp. 207–211, Eur. Space Agency, Paris.

Murphree, J. S., R. D. Elphinstone, L. L. Cogger, and D. Hearn (1991), Viking optical substorm signatures, in *Magnetospheric Substorms*, Geophys. Monogr. Ser., vol. 64, edited by J. R. Kan et al., pp. 241–255, AGU, Washington, D. C.

Murphree, J. S., R. D. Elphinstone, M. G. Henderson, L. L. Cogger, and D. J. Hearn (1993), Interpretation of optical substorm onset observations, *J. Atmos. Terr. Phys.*, 55, 1159–1170.

Pulkkinen, T. I., et al. (1991), Modeling the growth-phase of a substorm using the tsyganenko model and multi-spacecraft observations: CDAW-9, *Geophys. Res. Lett.*, 18, 1963–1966.

Reeves, G. D., and M. G. Henderson (2001), The storm-substorm relationship: Ion injections in geosynchronous measurements and composite energetic neutral atom images, *J. Geophys. Res.*, 106, 5833–5844.

Reeves, G. D., et al. (2004), IMAGE, POLAR, and geosynchronous observations of substorm and ring current ion injection, in *Disturbances in Geospace: Storm-Substorm Relationship*, *Geophys. Monogr. Ser.*, vol. 142, edited by A. S. Sharma, Y. Kamide, and G. S. Lakhina, pp. 91–101, AGU, Washington, D. C.

Singer, H. J., W. J. Hughes, P. F. Fougere, and D. J. Knecht (1983), Localization of Pi 2 pulsations: Ground-satellite observations, *J. Geophys. Res.*, *88*, 7029–7036.

Siscoe, G. L., N. U. Crooker, and K. D. Siebert (2002), Transpolar potential saturation: Roles of region 1 current system and solar wind ram pressure, *J. Geophys. Res.*, *107*(A10), 1321, doi:10.1029/2001JA009176.

Siscoe, G. L., J. Raeder, and A. J. Ridley (2004), Transpolar potential saturation models compared, *J. Geophys. Res.*, *109*, A09203, doi:10.1029/2003JA010318.

Zhou, X.-Y., et al. (2003), Ring current intensification and convection-driven negative bays: Multisatellite studies, *J. Geophys. Res.*, *108*(A11), 1407, doi:10.1029/2003JA009881.

————————————

P. C. Brandt, Johns Hopkins University Applied Physics Laboratory, Laurel, MD 20723-6099, USA.

M. H. Denton, M. G. Henderson, G. D. Reeves, R. Skoug, and M. F. Thomsen, Mail Stop D-466, Los Alamos National Laboratory, Los Alamos, NM 87545, USA. (mghenderson@lanl.gov)

T. J. Immel and S. B. Mende, Space Sciences Laboratory, University of California, Berkeley, Berkeley, CA 94720-7450, USA.

H. J. Singer, NOAA Space Environment Center, Boulder, CO 80305, USA.